

1 **Enhanced understanding of dominant drivers of**
2 **Water Yield change across China through the**
3 **improved coupled carbon and water model**

4 Huilan Shen ^{1,2}, Hanbo Yang ^{1,2,*}, Changming Li ^{1,2,3}

5 ¹ Department of Hydraulic Engineering, Tsinghua University, Beijing 100084, China

6 ² State Key Laboratory of Hydrosience and Engineering, Tsinghua University, Beijing 100084, China

7 ³ School of Civil Engineering and Transportation, State Key Laboratory of Subtropical Building and
8 Urban Science, South China University of Technology, Guangzhou 510641, China

9 * Correspondence: Hanbo Yang (yanghanbo@tsinghua.edu.cn)

10

11

12 **Abstract:** The rapid environmental changes, including climate change, escalating
13 atmospheric CO₂ concentration ([CO₂]), and vegetation dynamics, have been
14 significantly impacting hydrological processes. Yet disentangling the respective
15 contributions of climate, vegetation, and [CO₂] change to water yield (WY)—
16 especially clarifying [CO₂]-driven physiological effects—remains difficult. Therefore,
17 this study improved the coupled carbon and water (CCW) model integrating dynamic
18 water use efficiency (WUE) better capture CO₂-physiological feedbacks.; Using
19 scenario analysis, WY changes across China from 1982 to 2017 were attributed to
20 climate, vegetation, and [CO₂] drivers. The results showed that climate change
21 (especially precipitation change) emerged as the dominant driver, directly affecting
22 over 70% of China's land area. The vegetation change was the second largest factor to
23 reduce WY, especially in central China. The effect of the escalating [CO₂] was
24 relatively small. Spatial analysis aligned with isohyetal lines further revealed that
25 vegetation change and [CO₂] exerted greater influence within the 400–1600 mm
26 precipitation range. In addition, the elasticity analysis showed that the sensitivity
27 ranking of impact factors is precipitation > [CO₂] > NDVI for the whole China.
28 Therefore, CMIP6 SSP585 projections indicate that accelerating [CO₂] rise will
29 amplify its hydrological effect to a +1.29% annual WY increase by 2100, surpassing
30 vegetation influences. This study refines WY attribution by coupling dynamic WUE
31 with ecohydrological modeling, valuable insights for optimizing regional water
32 resource allocation and developing adaptive ecosystem management strategies under
33 future climate scenarios.

34 **Keywords:** the coupled carbon and water (CCW) model; WY change; climate change;
35 vegetation change; increasing atmospheric CO₂ concentrations; attribution analysis

36 **Plain language:** Climate change, rising CO₂, and vegetation dynamics are reshaping
37 global water cycle, but their impacts remain unclear. We improved the coupled carbon
38 and water model to analyze China's water yield (WY) changes (1982–2017). Our
39 results showed that climate change was the dominant driver nationally, vegetation/ CO₂

40 most affected in 400-1600 mm precipitation zones. Projections indicate CO₂ may
41 increase WY 1.3% annually by 2100, surpassing other drivers. This work informs
42 sustainable water management.

43 **1 Introduction**

44 The global environment has been undergoing rapid changes, impacting
45 hydrological processes through climate change, escalating atmospheric CO₂
46 concentration [CO₂], and vegetation dynamics (Piao et al., 2007; Wei et al., 2024).
47 Notably, China has experienced a visible greening trend in recent decades, prompting
48 a heightened focus on ecological and water resource concerns (Chen et al., 2019).
49 Investigating the influence of vegetation changes on runoff has thus emerged as a
50 pivotal research area, aligning with China's increasing emphasis on environmental
51 sustainability. China's diverse climatic zones and pronounced greening make it an ideal
52 natural laboratory for investigating these ecohydrological feedbacks, with insights that
53 are globally relevant yet directly informative for sustainable water resource
54 management and ecological restoration in China(Ogutu et al., 2021; Yang et al., 2019),
55 and for other semi-arid and monsoon-influenced regions such as the Sahel, South Asia,
56 and the Mediterranean Basin(Nkiaka et al., 2025; Rahman et al., 2025; Serrano-Notivoli
57 et al., 2022). Understanding the intricate interplay among vegetation dynamics, climate
58 change, and [CO₂] within the water cycle, particularly concerning runoff therefore it is
59 not only of global relevance but also of profound importance for advancing sustainable
60 water resource management and ecological restoration strategies in China under
61 accelerating environmental change

62 Several methods have been employed to separate the effects of climate, vegetation,
63 and [CO₂] change on runoff change, including paired catchment experiments, statistical
64 methods, and modeling approaches (Zeng et al., 2020). Given that annual water yield
65 (WY) equates to runoff through negligible soil water storage changes, these
66 methodological evaluations directly inform WY attribution frameworks (Zhang et al.,
67 2022b). The paired catchment experiment method, though classical, is limited to small-
68 scale watersheds and is less applicable to larger regions (Peng et al., 2016). Statistical
69 methods, while helpful in identifying correlations, lack a physical basis and are
70 insufficient for explaining the underlying mechanisms of runoff changes (Chen et al.,

71 2022). Modeling approaches for attribution fall into two broad classes: (i) process-
72 based models that explicitly simulate coupled water–energy–carbon processes, and (ii)
73 conceptual models that approximate these processes with parsimonious, physically
74 interpretable relationships (Zhai and Tao, 2021). Process-based models can capture
75 detailed mechanisms, but they require extensive inputs and many parameters, are
76 sensitive to calibration and equifinality, and are computationally demanding—
77 limitations that hinder basin-to-continental applications over long periods(Jiao et al.,
78 2017; Ma et al., 2023). By contrast, conceptual models retain key ecohydrological
79 mechanisms with far fewer parameters, scale well to large regions, and thus are well
80 suited for large-scale attribution while preserving physical interpretability. Among
81 these conceptual models, the Budyko framework, widely used to separate climate
82 change effects on runoff, quantifies water balance through the aridity index
83 (PET/precipitation) and incorporates a catchment-specific parameter “n” representing
84 integrated land surface characteristics (e.g., vegetation, soil, topography) (Zhang et al.,
85 2022a, 2016a). However, most Budyko-based applications primarily emphasize
86 climate-driven attribution; vegetation and [CO₂] influences are typically introduced
87 only indirectly—by assigning temporal changes in “n” to vegetation(Tan et al., 2024;
88 Xue et al., 2022; Zhou et al., 2023) or correlating “n” with NDVI (Liu et al., 2024; Tan
89 et al., 2023), and by embedding [CO₂] effects through PET adjustments(Liu et al., 2024).
90 — These practices conflate vegetation with other controls captured by “n” (e.g., soil,
91 topography) and mix [CO₂]-physiological impacts with meteorological drivers in PET,
92 making it difficult to isolate vegetation structural change from [CO₂]-induced stomatal
93 adjustments and to ascribe mechanisms robustly (Gan et al., 2021).

94 Specifically, elevated [CO₂] reduces stomatal conductance—due to smaller
95 stomatal apertures and increased leaf resistance (Lammertsma et al., 2011; Xu et al.,
96 2016) which decreases transpiration fluxes (ET). At the same time, carbon assimilation
97 rate (GPP) may increase with higher [CO₂] availability, but this increase is often less
98 proportional to the reduction in water loss (Montibeller et al., 2022) The resulting

99 imbalance—lower water loss relative to carbon gain—thus leads to higher water-use
100 efficiency ($WUE = GPP / ET$). In particular, conventional frameworks that neglect
101 $[CO_2]$ -driven physiological feedbacks fail to represent the enhanced water-use
102 efficiency (WUE) of vegetation under elevated $[CO_2]$ conditions. This omission leads
103 to ambiguous attribution of runoff variations, as part of the reduction in
104 evapotranspiration induced by stomatal closure is often misinterpreted as a vegetation
105 structural effect rather than a $[CO_2]$ -induced physiological adjustment. Although
106 numerous studies have examined vegetation and climate controls on runoff, few have
107 explicitly incorporated the $[CO_2]$ –WUE feedback within a mechanistic framework.
108 Most existing approaches either completely ignore this feedback or treat it as a simple
109 empirical or linear relationship, rather than capturing its process-based influence on
110 hydrological responses.

111 The coupled carbon and water (CCW) model integrates hydrological and
112 ecological processes by mechanistically linking vegetation dynamics to water and
113 carbon fluxes through remote sensing-driven parameterization (Li et al., 2024b; Zhang
114 et al., 2021b, 2022b). Unlike the Budyko framework’s empirical parameter “n”—which
115 conflates vegetation effects with unaccounted catchment characteristics—the CCW
116 model links vegetation and hydrology through a single mechanistic chain. In this
117 framework, vegetation structure (NDVI/LAI) determines canopy absorption of
118 photosynthetically active radiation (FPAR) and hence gross primary production (GPP)
119 via light-use efficiency, while evapotranspiration (ET) is coupled to GPP through a
120 biome-specific underlying water-use efficiency (UWUE) term with vapor pressure
121 deficit (VPD) regulation. Nevertheless, the original CCW model, while robust in
122 capturing vegetation-climate interactions, adopts a static UWUE and does not account
123 for CO_2 -induced physiological changes, specifically long-term enhancements in water-
124 use efficiency (WUE) resulting from elevated $[CO_2]$, thereby limiting its capacity to
125 isolate $[CO_2]$ fertilization effects from vegetation structural and climatic influences
126 (Adams et al., 2020; Li et al., 2023).

127 To address this limitation, our study enhanced the CCW framework by
128 incorporating dynamic WUE responses to [CO₂], allowing explicit attribution of runoff
129 changes to three distinct drivers—climate change (eg. precipitation, temperature, and
130 so on), vegetation structural change (NDVI, and land use and land cover (LULC)), and
131 [CO₂]-physiological effects (stomatal optimization). This extension advances beyond
132 empirical or regression-based attribution, clarifies how [CO₂] modulates vegetation–
133 hydrology interactions across large spatial scales, and provides policy-relevant
134 evidence for sustainable water resource management and ecological restoration in
135 China under accelerating environmental change. .

136 **2 Methods and Data**

137 **2.1 Data sources and processing**

138 Four main datasets were employed in the improved CCW model: vegetation data
139 (NDVI), climate data (precipitation, temperature, shortwave radiation, vapor pressure
140 deficit, and atmospheric pressure), land use and land cover (LULC), and [CO₂]. The
141 monthly NDVI dataset used in this study (Table 1) was derived from a daily 0.05° gap-
142 free NDVI dataset in China (<https://doi.org/10.6084/m9.figshare.c.7002225.v1>) (Li et
143 al., 2024a), which was developed from the NOAA’s daily NDVI dataset, applying
144 effective data recognition and spatiotemporal gap-filling techniques. The dataset spans
145 1981–2023 and provides a spatial resolution of 0.05°, and we used bilinear interpolation
146 to generate the dataset with a spatial resolution of 0.1°.

147 Climate data (Table 1), including precipitation, air temperature, surface downward
148 shortwave radiation, relative humidity, and atmospheric pressure, were sourced from
149 the China Meteorological Forcing Dataset (CMFD) at the National Tibetan Plateau
150 Data Center (TPDC) of the Institute of Tibetan Plateau Research, Chinese Academy of
151 Sciences (He et al., 2020). The dataset spans 1979–2018 and provides a spatial
152 resolution of 0.1° and temporal resolutions at 3-hour, daily, monthly, and annual scales.
153 As the dataset did not provide vapor pressure deficit (VPD), we calculated VPD using

154 the method from Howell and Dusek (1995), based on atmospheric pressure, temperature,
155 and relative humidity.

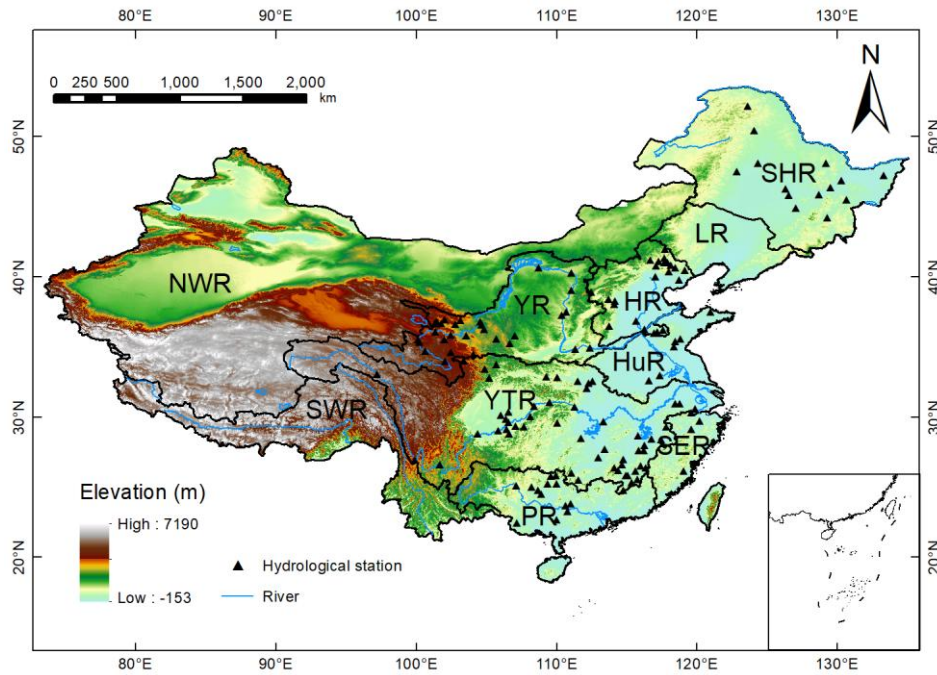
156 LULC data (Table 1) were obtained from the Zhang et al. (2024) global dataset,
157 which provides consistent multi-temporal global LULC maps at 30 m spatial resolution
158 for 1985–2022. The dataset includes 35 fine-resolution LULC types. For the purposes
159 of this study, and to facilitate LULC change analysis, we merged these 35 LULC types
160 into 17 types using the IGBP classification, based on the method by Yang et al. (2017).
161 Four primary LULC types—cropland, forest, grassland, and bare land—were
162 determined following the method described by Mu et al. (2013). The data were
163 resampled to the 0.1° spatial resolution, ensuring compatibility for modeling within the
164 modified CCW framework.

165 [CO₂] data were sourced from the Mauna Loa Observatory (MLO), Hawaii (20°N,
166 156°W) (<http://cdiac.esd.ornl.gov/ftp/trends/co2/maunaloa.co2>), with yearly
167 observations used to represent national [CO₂] levels due to the minimal spatial variation
168 in [CO₂] across China (Table 1). These datasets were then used to drive the improved
169 CCW model.

170 In this study, the hydrological data for model validation from 145 hydrological
171 stations (Fig. 1), each with at least 15 years of continuous data since 1982, was collected
172 from the Hydrological Bureau of the Ministry of Water Resources of China
173 (<https://www.mwr.gov.cn/english/>). Annual runoff data were calculated from the daily
174 runoff and the catchment area controlled by each hydrological station.

175 **Table 1.** Hydrology, climate, and vegetation data for the improved CCW model

Dataset	Original Resolution (spatial/temporal)	Period	Reference
NDVI	0.05° × 0.05° (daily)	1981 - 2023	(Li et al., 2024a)
Landcover	30m×30m (5-year)	1985 - 2022	(Zhang et al., 2024)
Climate	0.1° × 0.1° (monthly)	1979 - 2018	(He et al., 2020)
[CO ₂]	yearly	1959 - 2023	Mauna Loa Observatory, Hawaii



176

177 **Figure 1.** The geographic location and topography of the study area, where the black triangles
 178 mark the location of the hydrological gauging stations for model evaluation. Ten river basins
 179 considered in this study are: Songhua River basin (SHR), Liao River basin (LR), Hai River
 180 basin (HR), Huai River basin (HuR), Yangtze River basin (YZR), Yellow River basin (YR),
 181 Pearl River basin (PR), Southeast Rivers (SER), Southwest Rivers (SWR) and Northwest
 182 Rivers (NWR).

183 2.2 The improved CCW model

184 The original Coupled Carbon and Water (CCW) model (Zhang et al., 2016b) is a
 185 data-driven, remote sensing-based model that effectively integrates carbon and water
 186 dynamics to estimate monthly gross primary productivity (GPP) and evapotranspiration
 187 (ET). This model, which is particularly carbon-centric, derives ET from GPP
 188 constrained by underlying water-use efficiency (UWUE) parameters, which were
 189 calibrated using global FLUXNET data (Zhang et al., 2016b; Zhou et al., 2014). Despite
 190 its simpler structure, the CCW model achieves accuracy comparable to more complex
 191 process-based models in ET estimation. The essential components of the CCW model
 192 are represented as:

$$193 \quad GPP = APAR \times \varepsilon = PAR \times FPAR \times \varepsilon_{pot} \times R_s \times T_s \times W_s \quad (1)$$

194 where APAR is the absorbed photosynthetically active radiation (MJ m^{-2}), which is
 195 calculated as the product of incident photosynthetically active radiation (PAR) and the
 196 fraction of PAR absorbed by vegetation (FPAR), and PAR is typically assumed to be
 197 45% of the total shortwave radiation (Running et al., 2000); FPAR is determined by the
 198 normalized difference vegetation index (NDVI) (Sims et al., 2005); ϵ is the realized
 199 light-use efficiency (g C MJ^{-1}), which is calculated by multiplying the potential light-
 200 use efficiency (ϵ_{pot}) and environmental scalars for diffuse radiation (R_s), temperature
 201 (T_s), and moisture stress (W_s). This formulation ensures that GPP estimates reflect the
 202 influence of radiation, temperature, and moisture limitations on photosynthetic activity.

203 In this study, we improve the CCW model by incorporating dynamic water use
 204 efficiency (WUE) instead of static UWUE. This enhancement addresses the limitations
 205 of the original model, particularly its inability to adapt to environmental changes such
 206 as varying $[\text{CO}_2]$ and vapor pressure deficit (VPD). WUE's estimation method is
 207 estimated using the WEC (Water Efficiency and Carbon) equation proposed by Cheng
 208 et al. (2017). The final formula for calculating WUE is:

$$209 \quad WUE = \frac{C_a \times P_a}{1.6(\text{VPD} + g_1\sqrt{\text{VPD}})} [1 - \exp(-k * \text{LAI})](1 - f_i) \quad (2)$$

210 where C_a is atmospheric CO_2 concentration ($\text{mol}(\text{CO}_2) \text{ mol}^{-1}(\text{air})$); P_a is atmospheric
 211 pressure (kPa); VPD is vapor pressure deficit (kPa); g_1 is an empirical parameter of the
 212 Ball stomatal conductance model; k is the radiation extinction coefficient, typically set
 213 at 0.6, describing how light is absorbed by the canopy; LAI is the leaf area index; and
 214 f_i is a factor representing nonproductive water use (such as evaporation from soil and
 215 canopy interception). This equation provides a dynamic estimate of WUE, considering
 216 the effects of environmental factors like VPD, CO_2 concentration, atmospheric pressure,
 217 and canopy structure (LAI). The factor $1 - \exp(-k \times \text{LAI})$ accounts for light interception
 218 by the canopy. In this study, the interception evaporation factor (f_i) was set to zero.
 219 This simplification follows previous large-scale ecohydrological studies (Cheng et al.,
 220 2017), which reported that canopy interception and soil surface evaporation account for

221 a minor portion of total evapotranspiration at annual to multi-decadal scales. Given that
222 the improved CCW model focused on yearly water yield (WY) dynamics rather than
223 event-scale hydrological responses, neglecting interception loss reduces model
224 complexity without substantially affecting WY estimation.

225 In order to ensure the consistency of NDVI and LAI trends, we calculated LAI
226 using NDVI (Gutman and Ignatov, 1998) instead of LAI dataset:

$$227 \quad \left\{ \begin{array}{l} LAI = -2\ln(1 - f_{NDVI}) \\ f_{NDVI} = \frac{NDVI - NDVI_0}{NDVI_1 - NDVI_0} \end{array} \right. \quad (3)$$

228 where $NDVI_0 = 0.04$, $NDVI_1 = 0.52$

229 Evapotranspiration (ET) is then calculated as the ratio of GPP to WUE:

$$230 \quad ET = \frac{GPP}{WUE} \quad (4)$$

231 This modification allows the model to estimate ET using dynamic WUE, replacing the
232 static UWUE from the original model. The dynamic nature of WUE enhances the
233 model's ability to simulate ecosystem water use across different environmental
234 conditions and vegetation types.

235 Finally, the water yield (WY) is calculated as the difference between precipitation
236 (P) and ET:

$$237 \quad WY = P - ET \quad (5)$$

238 On an annual scale, WY is assumed to be approximately equal to runoff, as
239 changes in soil water storage over long periods (one year or longer) are considered
240 negligible (Xiao et al., 2020; Zhang et al., 2021b). Thus, the attribution of WY can also
241 be considered as the attribution of runoff. Accordingly, in this study WY is used as the
242 modelled output, while the term 'runoff' is reserved for observed streamflow or
243 literature values explicitly labelled as such.

244 **2.3 Attribution analysis framework**

245 To explore the combined and individual effects of climate, vegetation, and [CO₂]
 246 change on water yield (WY), four scenarios were designed based on data from 1982 to
 247 2017 (Table 2). Scenario 1 (Actual) aimed to validate the improved CCW model and
 248 estimate the combined effects of climate, vegetation, and [CO₂] change on WY by
 249 allowing all variables to vary from 1982 to 2017. Scenario 2 (Vegetation Change)
 250 focused on estimating the direct effects of vegetation change on WY by allowing
 251 vegetation variables (NDVI and LULC) to vary while keeping climate and [CO₂] fixed
 252 at 1982 levels. In this case, the trend in WY obtained reflects the impact of vegetation
 253 change alone. Scenario 3 (Climate Change) aimed to estimate the direct effects of
 254 climate change on WY by allowing climate variables (precipitation, temperature,
 255 relative humidity, solar radiation, and atmospheric pressure) to change, while fixing
 256 vegetation and [CO₂] at 1982 levels. This scenario helps isolate the effects of climate
 257 change on WY. Scenario 4 ([CO₂] Change) was designed to estimate the direct effects
 258 of [CO₂] change on WY by varying [CO₂] levels from 1982 to 2017, while climate and
 259 vegetation variables were fixed at 1982 levels. The resulting WY trend reflects the
 260 impact of [CO₂] change alone. The resulting WY series under each scenario represents
 261 the isolated impact of the corresponding driver.

262 **Table 2.** Scenario designs in the improved CCW model for WY attribution. LULC: Land use
 263 and land cover types; NDVI: Normalized difference vegetation index; TMP: Temperature;
 264 SRAD: Shortwave radiation; VPD: Vapor pressure deficit.

Scenarios	Vegetation		Climate				CO ₂	Purposes	
	LULC	NDVI	P	T	RH	Srad	Pa		CO ₂
S1 (baseline)	▲	▲	▲	▲	▲	▲	▲	▲	Validating the improved CCW model and estimating the combined effects of climate,

									vegetation, and CO ₂ change.
S2 (vegetation)	▲	▲	△	△	△	△	△	△	Estimating the direct effects of vegetation change.
S3 (climate)	△	△	▲	▲	▲	▲	▲	△	Estimating the direct effects of climate change.
S4 (CO ₂)	△	△	△	△	△	△	△	▲	Estimating the direct effects of CO ₂ change.

265 Note: The symbol “▲” denotes a changing input variable over time, whereas the symbol “△”
 266 represents a fixed input variable at the level of the initial year (1982).

267 For each scenario, the long-term trend in annual WY over 1982–2017 was
 268 quantified using the Theil–Sen estimator, yielding a robust slope. The relative
 269 contributions of climate, vegetation, and [CO₂] to changes in WY were calculated using
 270 the following formula (Ma et al., 2023; Wang et al., 2022):

$$271 \left\{ \begin{array}{l} RC_{vegetation} = \frac{trend_{vegetation}}{|trend_{vegetation}| + |trend_{climate}| + |trend_{CO_2}|} \times 100\% \\ RC_{climate} = \frac{trend_{climate}}{|trend_{vegetation}| + |trend_{climate}| + |trend_{CO_2}|} \times 100\% \\ RC_{CO_2} = \frac{trend_{CO_2}}{|trend_{vegetation}| + |trend_{climate}| + |trend_{CO_2}|} \times 100\% \end{array} \right. \quad (6)$$

272 where $trend_{vegetation}$, $trend_{climate}$, and $trend_{CO_2}$ represent the changes in water
 273 yield (WY) resulting from vegetation, climate, and [CO₂] changes, respectively, as
 274 calculated in each scenario; the relative contributions ($RC_{vegetation}$, $RC_{climate}$, and
 275 RC_{CO_2}) are expressed as percentages, indicating the proportion of each factor's
 276 influence on the overall changes in WY.

277 At each grid point, the absolute values of the relative contributions of each factor
 278 (vegetation, climate, and [CO₂]) are compared. For each grid point, we identify the
 279 most significant contributor to water yield (WY) changes by comparing the relative
 280 contributions of each factor. If the absolute values of the relative contributions of two

281 factors do not exceed 5%, then these two factors are considered joint significant
282 contributors to the changes in WY at that grid point (Jia et al., 2022). This approach
283 helps to highlight areas where the impacts of multiple factors are closely intertwined
284 and both play a critical role in influencing water yield, suggesting that their combined
285 effects are comparable in magnitude. In these cases, the relative contribution of each
286 factor is not significantly stronger than the other, indicating that their combined
287 influence on WY is equally important at the local scale.

288 The scenario analysis previously conducted revealed the relative contributions of
289 climate, vegetation, and [CO₂] to WY changes. However, these contributions arise from
290 both the intrinsic rate of change of each factor and the sensitivity of runoff to those
291 changes (the elasticity coefficient) (Yang and Yang, 2011). To gain a deeper
292 understanding of the changes in WY, we employ elasticity coefficients to quantify its
293 sensitivity to individual factor. We specifically focused on precipitation because,
294 despite not always having the highest sensitivity, it is integral to the hydrological cycle
295 and essential for assessing water yield (WY) under various climate change scenarios
296 (Liu et al., 2017). The elasticity of runoff refers to the variation in runoff depth resulting
297 from a 1% increase in each climatic variable (Xu et al., 2014). The absolute value of
298 elasticity reflects the sensitivity of runoff to various influencing factors. In other
299 methods, elasticity coefficients are typically calculated using an analytical expression
300 based on instantaneous changes in runoff corresponding to variations in a given factor
301 in a specific year (Fu et al., 2023; Liu et al., 2017; Yang and Yang, 2012). However, in
302 our study, we applied scenario-based analysis over the period of 1982 to 2017. This
303 extended temporal window allowed us to better account for the long-term effects and
304 interactions of multiple factors influencing WY. So we vary each factor (precipitation,
305 NDVI, and [CO₂]) by 1% relative to the baseline scenario S1 across the entire 1982-
306 2017 period. We then calculated the annual average runoff values from the adjusted
307 sequence and compared them with the average original baseline runoff values. The

308 difference between these two values, divided by the average baseline runoff value, gave
309 us the runoff change rate:

$$310 \quad \frac{\Delta R_x}{R_x} = \frac{WY_{mean_x} - WY_{mean_x}}{WY_{mean_x}} \quad (7)$$

311 Mathematically, the elasticity coefficient is defined as the runoff change rate
312 divided by 1%, and the formula is as follows:

$$313 \quad \varepsilon_x = \frac{\frac{\Delta R_x}{R_x}}{\frac{\Delta x}{x}} = \frac{\frac{\Delta R_x}{R_x}}{1\%} \quad (8)$$

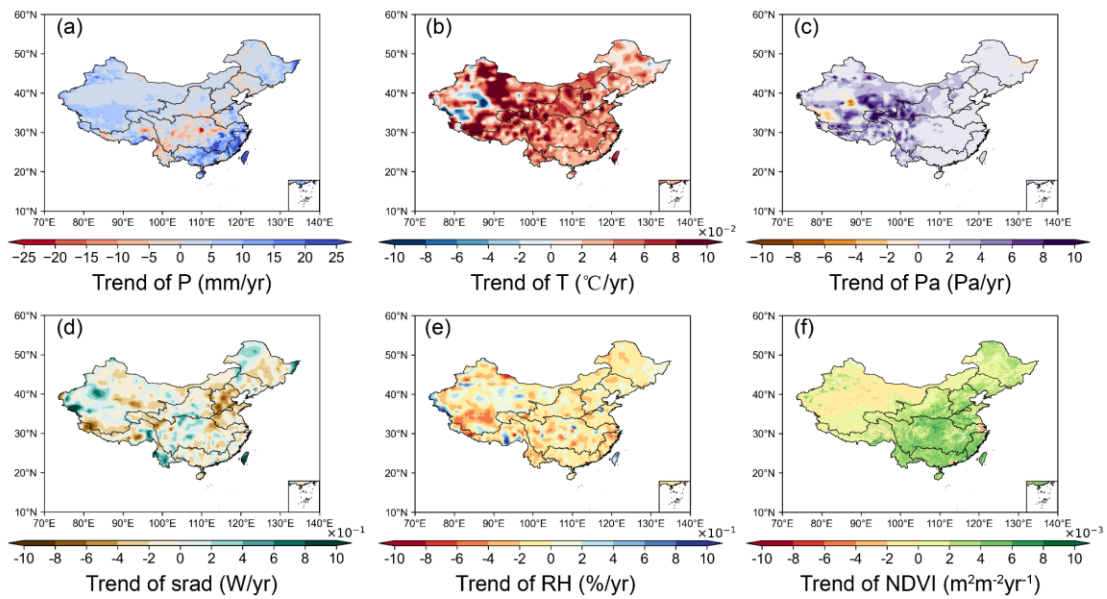
314 Generally, while the scenario analysis above has identified which factors are most
315 influential based on their relative contributions, the elasticity coefficients allow us to
316 explain why these factors are critical by demonstrating their respective impacts on WY
317 through sensitivity analysis. This dual approach—combining both the changes in the
318 factors and their elasticities—provides a more comprehensive understanding of the
319 drivers behind the observed changes in WY, ensuring that the results of the scenario
320 analysis are both meaningful and robust.

321 **3 Results**

322 **3.1 Changes in hydrometeorological variables**

323 Fig. 2 demonstrates the trends of annual precipitation, air temperature, relative
324 humidity, atmospheric pressure, solar radiation, and NDVI across China during 1982-
325 2017. Annual precipitation change exhibited a clear spatial distribution pattern,
326 specifically decreases in central China, including the middle reaches of the Yellow
327 River and the Yangtze River basins, and increases in the northwest and southeast. Air
328 temperature exhibited a consistent warming trend across China. In contrast, relative
329 humidity generally decreased across most China. Atmospheric pressure remained
330 relatively stable. Regarding solar radiation, decreases were in northern China, while an
331 increase was in southern regions. The decreasing solar radiation in northern China is

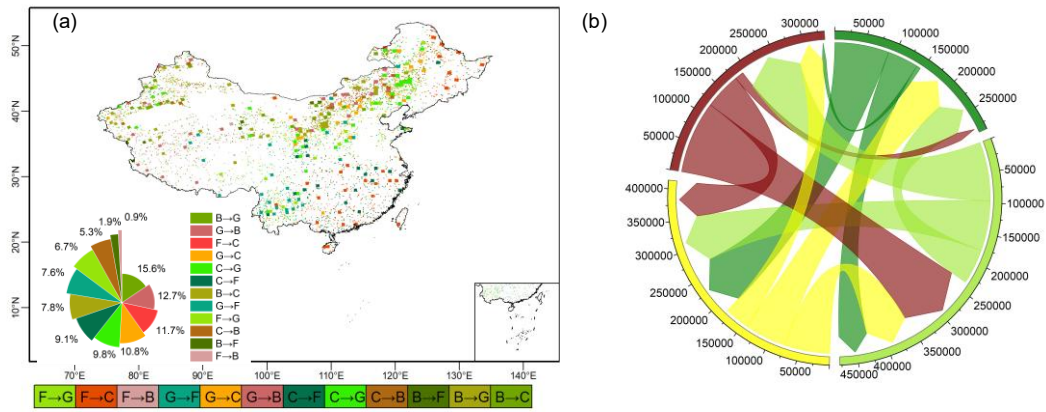
332 likely due to increased aerosol concentrations (Liang et al., 2024). NDVI showed a
 333 significant increasing trend, which indicates an overall enhancement in vegetation
 334 growth across China. This trend was especially prominent in central and eastern regions,
 335 including the Yellow River Basin and the Yangtze River Basin. In these regions, LULC
 336 changes, such as afforestation and agricultural practices, likely contributed to the
 337 observed increases in NDVI (Chen et al., 2019).



338
 339 **Figure 2.** Spatial patterns of trends in annual climatic and vegetation variables during 1982–
 340 2017. (a) precipitation (mm/yr); (b) air temperature ($^{\circ}\text{C}/\text{yr}$); (c) Atmospheric pressure (Pa/yr);
 341 (d) shortwave radiation ($\text{W}/\text{m}^2/\text{yr}$); (e) relative humidity ($\%/ \text{yr}$); (f) NDVI ($\text{m}^2\text{m}^{-2}\text{yr}^{-1}$).

342 Significant changes in land use and land cover (LULC) occurred in China during
 343 1982-2017, as illustrated in Fig. 3. Although the overall percentage distribution of
 344 major land cover types, namely grasslands, forests, croplands, and bare lands, remained
 345 relatively stable, these four categories dominated the landscape, with most changes
 346 concentrated within them. Notably, the transitions among these categories were
 347 characterized by mutual conversions, particularly from bare land to grasslands (Fig. 3).
 348 Spatially, the changes exhibited distinct regional patterns. In southern China, LULC
 349 changes were mainly characterized by the conversion of land to forests and grasslands.
 350 In contrast, the northeastern regions exhibited more complex transformations, with
 351 some areas shifting to bare land and croplands (Fig. 3).

352



353

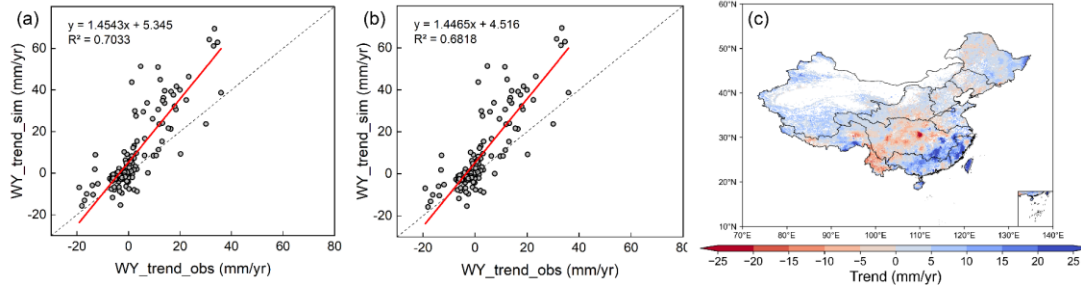
354 **Figure 3.** Land use and land cover (LULC) changes from 1982 to 2017. (a) Spatial pattern
 355 distribution of LULC change; (b) Chord diagram of LULC conversion flows (unit: km²), where
 356 directional arrows represent transitions between land types (originating type → current type),
 357 with chord widths proportional to the converted areas. The figure illustrates the converted areas
 358 and does not include the unchanged regions.

359 **3.2 Performance of the improved CCW model**

360 As shown in Fig. 4a and b, the observed annual water yield (WY) and the
 361 simulated annual WY by the improved CCW model showed strong linear correlations
 362 ($R^2 = 0.7$), with the regression line slope being 1.45, R^2 being 0.7, and RMSE being
 363 9.54 mm/year. By contrast, the initial model without WUE showed weaker skill (slope
 364 = 1.45, $R^2 = 0.68$, $RMSE = 9.62 \text{ mm} \cdot \text{yr}^{-1}$), indicating that explicitly representing [CO₂]-
 365 induced regulation of water-use efficiency measurably improves accuracy and reduces
 366 bias.

367 The estimated annual WY trends had distinct spatial patterns (Fig. 4c), which
 368 closely aligned with that of precipitation. Specifically, decrease trends in WY occurred
 369 in the central regions of the Yellow River Basin and the middle section of the Yangtze
 370 River Basin, while increase trends were found in other regions, with the southeast
 371 exhibiting the highest rate of increase.

372

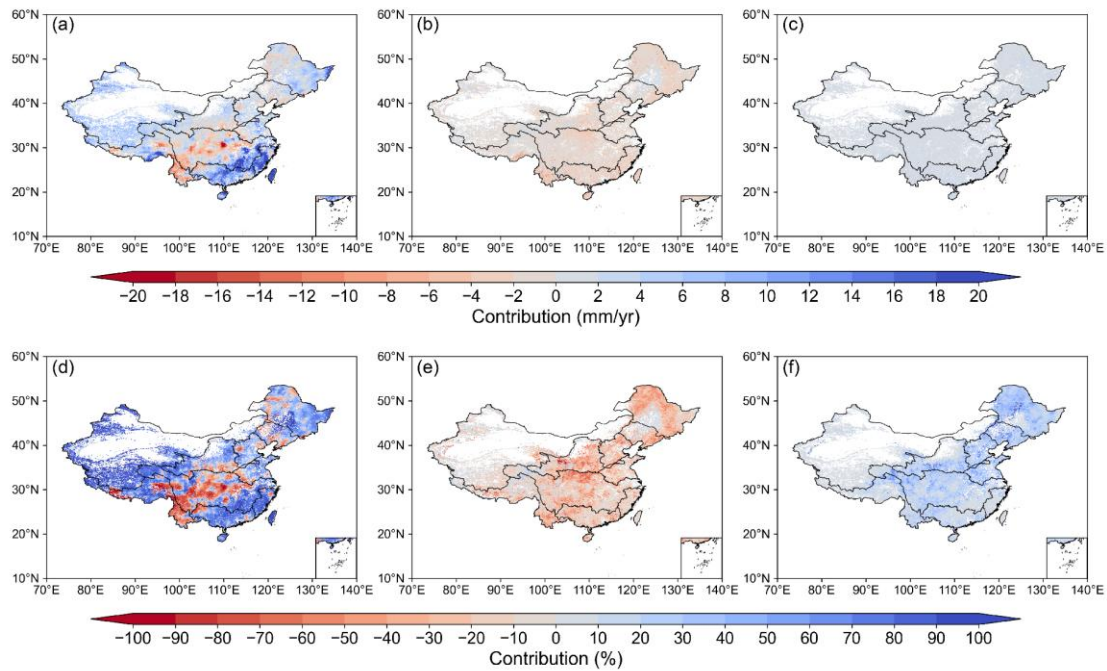


373

374 **Figure 4.** (a) Validation of simulated WY trend using the improved CCW model; (b) Validation
 375 of simulated WY trend using the initial CCW model; (c) Spatial distribution of WY trends
 376 under scenario S1(actual situation) during 1982–2017.

377 **3.3 Attribution analysis of annual WY changes**

378 Fig. 5 shows the distribution of WY changes caused by climate, vegetation, and
 379 [CO₂] changes, integrating both absolute magnitude (Fig. 5a-c) and relative dominance
 380 (Fig. 5d-f) of their contributions. Climate-driven WY changes exhibited marked spatial
 381 heterogeneity, with absolute increases exceeding 15 mm/yr in southeastern China (Fig.
 382 5a), corresponding to 60-90% relative contributions (Fig. 5d). Central basins showed
 383 contrasting declines of 0-6 mm/yr under climate forcing, while northeastern transitional
 384 zones displayed mixed positive/negative absolute changes (Fig. 5a) despite maintaining
 385 40-70% relative climate dominance (Fig. 5d). This spatial heterogeneity aligned with
 386 precipitation change patterns (Fig. 2a).



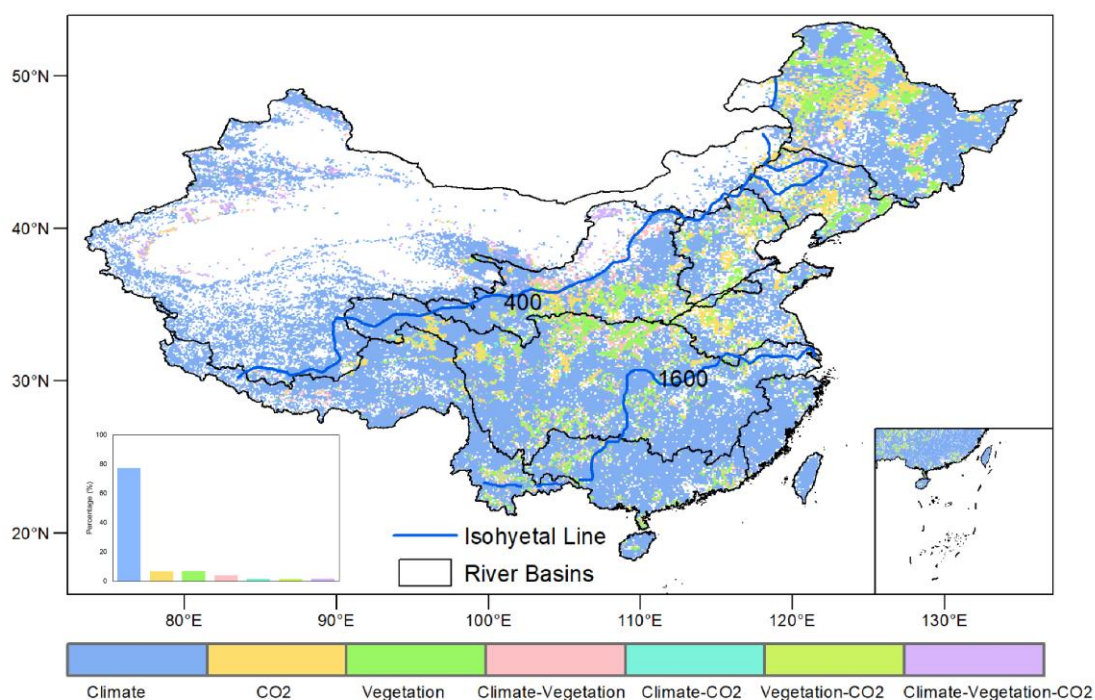
387

388 **Figure 5.** The absolute contributions of (a) climate, (b) vegetation, and (c) [CO₂], and the
 389 relative contributions of (d) climate, (e) vegetation, and (f) [CO₂] to changes in WY trends for
 390 1982-2017.

391 Vegetation-mediated WY reductions reached 0-6 mm/yr (Fig. 5b), accompanied
 392 by 0-60% relative contributions (Fig. 5e). These effects originated from enhanced
 393 evapotranspiration through land-use changes and NDVI-based greening, particularly
 394 pronounced in central China. Specific regions in the Yangtze, Yellow, and northeastern
 395 rivers showed vegetation-driven relative contributions reaching 40-60% (Fig. 5e). [CO₂]
 396 effects generated limited direct absolute impacts (<5 mm/yr, Fig. 5c) but exerted 10-
 397 40% relative influences (Fig. 5f) through stomatal closure mechanisms. This process
 398 partially counteracted vegetation-related WY losses in transitional climates like
 399 northeastern China, where competing drivers created complex ecohydrological
 400 interactions (Fig. 5d-f).

401 Fig. 6 illustrated the spatial distribution of WY trend drivers over the past four
 402 decades. Climate change was the dominant factor of WY variation in more than 70%
 403 regions, mainly in the Northwest, Southwest, Southeast, Pearl River basins, and other
 404 parts of the Yangtze and Yellow River basins. Vegetation changes ranked as the
 405 secondary control, dominating WY changes in parts of the Yangtze, Yellow, Songhua,

406 Liao, and Hai Rivers. Remarkably, it was shown that the region where vegetation and
 407 [CO₂] had the dominant influence mainly distributes within precipitation ranges of 400–
 408 1600 mm. CO₂-induced effects were least influential at a national scale. This three-
 409 tiered hierarchy—climate changes as the primary forcing, vegetation changes as the
 410 secondary control, and [CO₂] effects as a localized modifier—reveals how hydrological
 411 regimes govern the spatial succession of dominant drivers across China's diverse
 412 ecohydrological gradients.

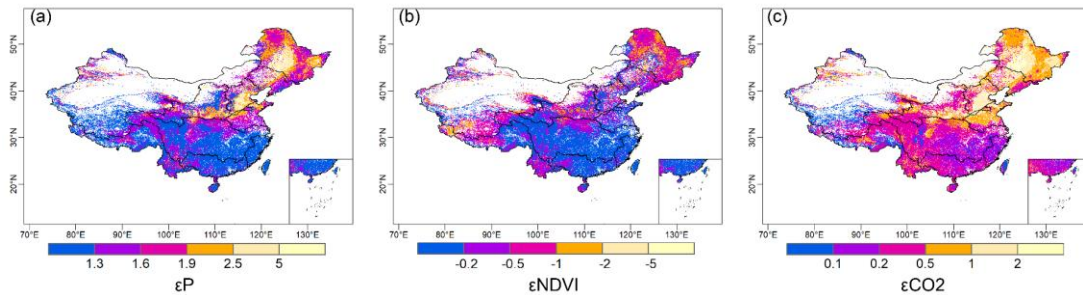


413

414 **Figure 6.** Spatial distributions of dominant factors controlling WY change. Driving factors
 415 include climate, vegetation, and [CO₂]. Climate: Areas where climate (e.g., precipitation,
 416 temperature) is the dominant factor influencing WY change; CO₂: Areas where [CO₂]
 417 is the primary driver of WY change; Vegetation: Areas where vegetation changes (e.g.,
 418 NDVI, LULC) primarily drive WY changes. Climate-Vegetation: Areas where both climate
 419 and vegetation jointly influence WY; Climate-CO₂: Areas where both climate and [CO₂]
 420 jointly contribute to WY change; Vegetation-CO₂: Areas where vegetation changes and [CO₂]
 421 jointly control WY; Climate-Vegetation-CO₂: Areas where the combined effect of climate,
 422 vegetation, and [CO₂] jointly controls WY change. Additionally, the approximate isohyetal
 423 lines shown in the figure were derived based on annual precipitation data from 1982 to 2017.

424 3.4 Elasticity of WY to main variables

425 The sensitivity of WY to precipitation (ϵP), NDVI ($\epsilon NDVI$), and $[CO_2]$ (ϵCO_2)
426 exhibits distinct spatial patterns in (Fig. 7). Nationally averaged elasticity coefficients
427 showed that a 10% increase in precipitation, $[CO_2]$, and NDVI altered WY by 15.5%
428 ($\epsilon P=1.55$), 5.5% ($\epsilon CO_2=0.55$), and -4.4% ($\epsilon NDVI=-0.44$), respectively, indicating that,
429 in terms of the sensitivity of runoff to changes in each factor, the ranking was
430 precipitation > $[CO_2]$ > NDVI.



431

432 **Figure 7.** Spatial distribution of elasticity coefficients of WY relative to changes in
433 hydrological variables such as (a) annual precipitation, (b) NDVI, and (c) $[CO_2]$.

434 The elasticity coefficients of precipitation (ϵP), $[CO_2]$ (ϵCO_2), and vegetation
435 ($|\epsilon NDVI|$) all exhibited a coherent latitudinal decline across China's river basins,
436 showing systematically higher sensitivity in northern regions than southern
437 counterparts. Quantitatively, ϵP decreased from 2.09 in the Songhua River basin to 1.15
438 in the Southeastern Basin, accompanied by similar reductions in $|\epsilon NDVI|$ (from 0.76 to
439 0.13) and ϵCO_2 (from 1.08 to 0.16) (Table 3).

440 A distinct abrupt transition zone in elasticity coefficients was identified around
441 $33^\circ N$, closely aligning with China's traditional North-South physiographic divide.
442 Around the zone, elasticity coefficients exhibited an abrupt decline from the Yellow
443 River Basin to the Yangtze River Basin. Specifically, the Yellow River Basin showed
444 higher sensitivities to precipitation ($\epsilon P=1.87$), $[CO_2]$ ($\epsilon CO_2=0.86$), and NDVI
445 ($\epsilon NDVI=-0.53$), which were approximately 1.4, 2.8, and 2.8 times greater, respectively,
446 than those in the Yangtze River Basin ($\epsilon P=1.31$, $\epsilon CO_2=0.31$, $\epsilon NDVI=-0.19$).

447 **Table 3.** Elasticity Coefficients of Runoff to Precipitation, NDVI, and CO₂ in Different
 448 Watersheds

Dataset	ϵ_P	ϵ_{NDVI}	ϵ_{CO_2}
Songhua River basin	2.09	-0.76	1.08
Hai River basin	2.13	-0.44	1.12
Yellow River basin	1.87	-0.53	0.86
Yangtze River Basin	1.31	-0.19	0.31
Huai River basin	1.64	-0.18	0.63
Pearl River basin	1.25	-0.17	0.25
Southeast Rivers	1.15	-0.13	0.15

449 Note: Some LULC types were excluded from the analysis. Due to many missing data points,
 450 the Liao River, Southwest, and Northwest river basins were also omitted.

451 **4 Discussion**

452 **4.1 Strength of the attribution analysis framework**

453 To address limitations in current methods for analysing the effects of climate,
 454 vegetation, and [CO₂] on runoff changes, we developed an attribution analysis
 455 framework based on the improved CCW model. This framework has been improved in
 456 three aspects. Firstly, the explicit and mechanistic integration of vegetation dynamics
 457 and [CO₂] effects overcomes the oversimplifications inherent in conventional
 458 approaches. Traditional Budyko-based frameworks often attribute vegetation effects to
 459 temporal variations in the parameter "n" by either statistically regressing "n" against
 460 vegetation proxies such as NDVI (Liu et al., 2024; Tan et al., 2023) or simplistically
 461 equating "n" to vegetation effects (Li et al., 2020b; Zhou et al., 2023). Such approaches
 462 conflate structural vegetation changes (e.g., leaf area index) with physiological
 463 adjustments (e.g., CO₂-induced stomatal closure), thereby obscuring the independent
 464 roles of vegetation dynamics and [CO₂]. For example, while rising [CO₂] levels directly
 465 reduce stomatal conductance and transpiration, Budyko-based studies often
 466 misinterpret this effect as part of the "n" parameter's variability, erroneously attributing
 467 it to vegetation changes (Zeng et al., 2020). In contrast, our framework mechanistically
 468 separates these pathways by explicitly describing the stomatal conductance–WUE

469 relationship based on plant physiological theory. Elevated [CO₂] reduces stomatal
470 aperture, thereby lowering stomatal conductance and transpiration flux while only
471 modestly increasing carbon assimilation, leading to an overall enhancement in water-
472 use efficiency (WUE). This process is represented by the Medlyn-type stomatal
473 conductance model (Medlyn et al., 2011), which links photosynthetic rate (A),
474 transpiration (T), and vapor pressure deficit (D) as:

$$475 \quad \frac{A}{T} = \frac{C_a P_a}{1.6(D + g_1 \sqrt{D})}$$

476 where C_a is atmospheric CO₂ concentration, P_a is air pressure, D is vapor pressure
477 deficit, and g_1 is an empirical slope parameter that quantifies plant sensitivity to CO₂
478 and humidity. According to this formulation, rising [CO₂] increases while reducing
479 stomatal conductance, which in turn suppresses transpiration more strongly than
480 photosynthesis, resulting in higher WUE. This mechanistic representation enables our
481 framework to capture the direct physiological CO₂ effect on evapotranspiration, which
482 is otherwise masked in Budyko-type models where CO₂ impacts are embedded
483 implicitly in PET or the “n” parameter.

484 Secondly, unlike Budyko-based methods that indirectly represent [CO₂] impacts
485 through adjustments to potential evapotranspiration (PET)—a practice conflating [CO₂]
486 effects with meteorological drivers like radiation and wind—our framework explicitly
487 quantifies CO₂'s physiological influence on actual evapotranspiration (AET) by
488 mechanistically modeling its role in stomatal conductance and water-use efficiency
489 (WUE). Elevated [CO₂] reduces stomatal conductance and transpiration while
490 moderately enhancing carbon assimilation, partially offsetting water losses associated
491 with vegetation greening. For example, our results show that reduction in transpiration
492 due to CO₂-driven stomatal closure offsets water losses, a mechanism entirely masked
493 in Budyko frameworks where [CO₂] effects are ambiguously embedded in PET
494 adjustments or erroneously attributed to vegetation structural changes via the "n"
495 parameter (Liu et al., 2024). This coupled regulation clarified how water and energy

496 jointly constrain evapotranspiration, particularly in 400-1600 mm precipitation zones.
497 In these regions, vegetation growth enhanced transpiration and root water uptake until
498 increasing atmospheric aridity imposed physiological constraints, while rising [CO₂]
499 partially counteracted this effect by improving water-use efficiency through stomatal
500 closure. As a result, the framework provided a more mechanistically grounded
501 understanding of how CO₂ fertilization modulates ecosystem water use and
502 hydrological responses at regional scales. Thirdly, while numerous studies have
503 conducted runoff attribution analysis at the basin scale (Liu et al., 2024, 2017; Yang et
504 al., 2022), our grid-scale approach transcends the spatial constraints of fixed watershed
505 boundaries by resolving regional heterogeneity in hydrological drivers. Conventional
506 basin-aggregated methods obscure critical intra-basin differences—for instance, our
507 analysis reveals that grids in the upper Yangtze River basin, where precipitation change
508 dominates runoff trends, necessitate climate scenario-based water resource planning. In
509 contrast, mid-basin grids with significant NDVI-driven greening exhibit pronounced
510 WY reductions, highlighting the need for vegetation management strategies that restrict
511 excessive afforestation in water-sensitive areas (Sun et al., 2022; Yang et al., 2021). By
512 decoupling analysis from rigid watershed boundaries, our framework enables targeted
513 strategies such as restricting reforestation in water-stressed grids or selecting CO₂-
514 adapted vegetation species, thereby aligning management actions with localized
515 climate-vegetation-hydrology interactions.

516 **4.2 New insights into attribution analysis**

517 Our findings highlighted climate change as the dominant driver of water yield (WY)
518 changes (contributing >70%), consistent with other assessments (Table 4), yet reveal
519 critical regional divergences. Climate impacts dominated in the Northwest and
520 Southwest River Basins, as well as parts of the Yangtze, Yellow, Southeast, and Pearl
521 River Basins, while vegetation and [CO₂] effects prevailed in central China (parts of
522 the Yangtze, Yellow, Songhua, Liao, and Hai River basin)—a spatial pattern slightly

523 distinct from earlier studies. Although previous studies identified human activities as
 524 the primary driver in some northern basins (Liao, Hai, and Yellow River Basins) ((Yang
 525 et al., 2022), their long-term study (1965-2018) diluted the gradually strengthening
 526 vegetation signals after 2000 mentioned in other studies (Liu et al., 2017; Sun et al.,
 527 2023) through time-averaging. Our findings now confirm the emerging importance of
 528 vegetation dynamics in southern basins like the Yangtze through our symmetric 1982-
 529 2017 study period.

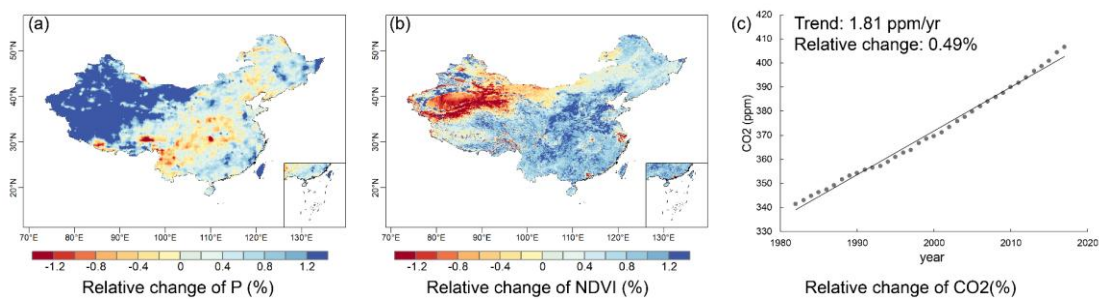
530 **Table 4.** Comparative studies of the contribution of climate variability and vegetation to runoff
 531 changes.

Reference	Study region	Study period	Method/Model	Driving factors
(Wei et al., 2024)	Global	1981-2020	Trendy phase 11 +ROF	Climate change
(Liu et al., 2024)	Global	1984-2010; 2000-2100	Improved Budyko	Precipitation
(Zhou et al., 2023)	Global	1850-2014; 2015-2100	Improved Budyko + CMIP6	Land surface changes
(Tan et al., 2023)	Global	2003-2016; 1982-2016	Improved Budyko	Effective precipitation
(Yang et al., 2022)	China	1965-2018	Budyko	P: Northwest river basin, Southwest river basin, Yangtze river basin, Southeast river basin, and Pearl river basin; n: Liaohe river basin, Haihe river basin, Yellow river Basin, Songhuajiang river basin, and Huaihe river basin
(Zhang et al., 2022b)	Yangtze River	2001-2018	CCW Model	Climate variability
(Chen et al., 2022)	Six river basins in China	1982-2015	Gray Relational Analysis (GRA)	Precipitation
(Zhai and Tao, 2021)	China	1982-2015	VIC Model	Climate change
(Li et al., 2020a)	Yihe River	1960-2013	SWAT+WRF	Climate variability
(Shen et al., 2017)	China	1960-2010	Budyko	Underlying surface change (n): the Songhua Basin, the Liaohe Basin and the Haihe Basin; Climate change: in other basins.

532 Elasticity analysis (Section 3.4) revealed distinct sensitivities of WY to
 533 environmental drivers: precipitation exhibited the highest elasticity coefficient for the
 534 whole China ($\epsilon_P = 1.55$), followed by CO_2 ($\epsilon_{CO_2} = 0.55$) and NDVI ($\epsilon_{NDVI} = -0.44$).

535 However, spatial analysis showed that vegetation and [CO₂] collectively dominated
 536 WY changes in 400–1600 mm/yr precipitation zones, despite their lower sensitivity
 537 rankings. The joint effect of elasticity and the magnitude of driver change that
 538 determines each driver’s net contribution. In the 400–1600 mm/yr precipitation zones,
 539 NDVI displayed (Fig. 8) a larger relative temporal variation compared with
 540 precipitation, which fluctuated within a narrower range.. Consequently, vegetation’s
 541 stronger relative change amplified its hydrological influence, overriding its lower
 542 elasticity. Similarly, CO₂’s historical impact was constrained by its slow accumulation
 543 rate (0.49%/yr), yet its relatively high elasticity positions it as a latent driver.

544



545

546 **Figure 8.** Spatial distribution of relative changes of different variables: (a) annual precipitation,
 547 and (b) NDVI.

548 This historical constraint, however, belied CO₂’s transformative potential under
 549 intensified forcing scenarios. CMIP6 SSP585 projections indicate [CO₂] will rise at
 550 2.34%/yr—nearly fivefold faster than historical rates (Cheng et al., 2022). At this
 551 trajectory, CO₂’s elasticity would drive a +1.29% annual WY increase, eclipsing both
 552 vegetation greening effects and even surpassing precipitation-driven changes in some
 553 regions. Such reversal underscores the imperative to prioritize [CO₂] in long-term water
 554 management, particularly in 400–1600 mm/yr precipitation zones.

555 From a policy perspective, these spatial contrasts have distinct implications for
 556 regional water management. In vegetation-dominated regions such as the Yangtze and
 557 Huang river basins, enhancing ecosystem-based restoration, optimizing vegetation
 558 composition, and preventing overgreening that may suppress runoff should be

559 prioritized. Conversely, in climate-dominated areas such as Northwest and Southeast
560 China, adaptive measures emphasizing precipitation variability, water storage capacity,
561 and drought resilience are crucial. Recognizing and tailoring water management
562 strategies to these driver-specific regimes can enhance the effectiveness of both
563 ecological restoration and climate adaptation programs across China.

564 **4.3 Uncertainty in attribution analysis**

565 This study provides valuable insights into the relationship between water resources
566 management and environmental changes, which can guide environmental management
567 strategies. However, several limitations exist that need to be addressed in future work
568 to improve the accuracy and robustness of the results.

569 Firstly, the improved CCW model does not account for the variation and specific
570 values of f_i , assuming f_i is 0. In reality, f_i represents the ratio of interception evaporation
571 to total evaporation, and in regions with abundant vegetation, f_i is not zero. Despite this,
572 considering the small change of f_i in the current year (Zhao et al., 2022), its influence
573 on runoff trends is negligible in our study (Cheng et al., 2017). However, future work
574 should prioritize its calculation to improve the precision of WY estimates.

575 Secondly, the complex interrelationships among climate, vegetation, and $[\text{CO}_2]$
576 cannot be fully disentangled. Vegetation exhibits tight biophysical interactions and
577 feedback with climate, making it difficult to separate the impacts of climate change,
578 vegetation dynamics, and $[\text{CO}_2]$ on hydrological responses. Changes in vegetation,
579 such as NDVI, reflect a combination of climate change, human activities (e.g.,
580 reforestation and irrigation), and natural vegetation growth. Additionally, vegetation
581 greening in upwind regions can increase atmospheric moisture, potentially enhancing
582 precipitation downwind (Zhang et al., 2021a), which may counteract some of the
583 negative impacts of increased evapotranspiration on local WY. Although the climate
584 data used in our model may implicitly capture some of these feedbacks, they cannot be
585 explicitly separated in this analysis. Consequently, our results represent an attempt to

586 estimate the direct first-order net impacts of climate, vegetation greening, and [CO₂]
587 increase on WY (Zhang et al., 2021b). Future research should adopt more
588 comprehensive models that consider soil-vegetation-atmosphere interactions to better
589 differentiate the contributions of each driving factor to WY.

590 Thirdly, the improved CCW model does not incorporate certain human activities,
591 such as large-scale irrigation, groundwater pumping, and reservoir regulation, which
592 should be incorporated in future studies. For instance, irrigation can sustain vegetation
593 greening during dry seasons, potentially amplifying the vegetation–climate feedback
594 on water yield. Incorporating such anthropogenic processes into the CCW framework
595 through coupled irrigation and water management modules would enable more
596 comprehensive attribution analyses in future studies. Our research also excludes water
597 bodies and built-up land. While urbanization can increase flood risks due to the growing
598 proportion of impervious surfaces (Wasko and Sharma, 2017), these land-use changes
599 represent a small portion of China’s land area.

600 Finally, the future impact of vegetation greening on hydrological dynamics will
601 depend on projected climate warming and drying trends, the persistence of vegetation
602 greening, [CO₂] changes, and the complex feedbacks between climate, soil, and
603 vegetation. These interactions require long-term study, and future research will involve
604 more extensive monitoring to better capture these evolving dynamics.

605 **5 Conclusions**

606 In this study, we improved the CCW model incorporating dynamic water use
607 efficiency (WUE) calculation to explicitly represent CO₂-physiological feedback on
608 water yield. This mechanistic improvement enabled comprehensive national-scale
609 assessment quantifying the relative contributions of climate forcing, vegetation
610 structural changes, and CO₂-driven stomatal regulation to water yield (WY) dynamics
611 in China. The main conclusions are as follows:

612 The improved CCW model effectively simulated WY variations in most basins
613 under increased [CO₂] scenarios, demonstrating its applicability and reliability in
614 modeling WY changes.

615 Climate change, particularly variations in precipitation, emerged as the primary
616 driver influencing WY, displaying significant regional disparities in its effects.
617 Vegetation changes constituted the second most critical factor, predominantly resulting
618 in WY reduction, notably in central China. While the effect of CO₂-induced stomatal
619 closure on WY was comparatively minor. Spatial analysis aligned with isohyetal lines
620 further revealed that vegetation change and [CO₂] exerted greater influence within the
621 400–1600 mm precipitation range.

622 The elasticity analysis of WY indicated that northern basins exhibit higher
623 sensitivity to influencing factors, whereas southern basins demonstrate relatively lower
624 elasticity. Specifically, the absolute elasticity coefficients for the whole China were
625 ranked in descending order as follows: precipitation > [CO₂] > NDVI. Thus,
626 accelerating [CO₂] rise (2.34% /yr under SSP585) will amplify its hydrological role,
627 potentially elevating CO₂-driven WY increases to +1.29% annually by 2100, surpassing
628 climate and vegetation impacts.

629 These insights provide a nuanced understanding of regional hydrological
630 responses, essential for sustainable water resource management under changing
631 environmental conditions.

632 **Acknowledgements**

633 This research was supported by the China National Key R&D Program (grant no.
634 2024YFF1306901).

635 **Data Availability Statement**

636 Datasets used for driving models were obtained from different sources described
637 in Table 1. All the data related to our results in this study can be found online: the NDVI

638 data (<https://doi.org/10.6084/m9.figshare.c.7002225.v1>); the climate data
639 (<https://www.tpdc.ac.cn/zh-hans/data/8028b944-daaa-4511-8769-965612652c49/>); the
640 land use and land cover (LULC) data (<https://zenodo.org/records/8239305>) (Liu et al.,
641 2023); and the [CO₂] (<http://cdiac.esd.ornl.gov/ftp/trends/co2/maunaloa.co2>), except
642 for the streamflow records for hydrological gauging stations, which are available upon
643 reasonable request.

644 **Author contributions**

645 HS designed the study, developed the model code, did the simulation experiments,
646 and wrote the first draft of the paper. HY designed the research and edited the
647 manuscript. CL provided feedback on the results and edited the manuscript.

648 **Competing interests**

649 The contact author has declared that neither they nor their co-authors have any
650 competing interests.

651

652 **Reference**

- 653 Adams, M. A., Buckley, T. N., and Turnbull, T. L.: Diminishing CO₂-driven gains in
654 water-use efficiency of global forests, *Nat. Clim. Chang.*, 10, 466–471,
655 <https://doi.org/10.1038/s41558-020-0747-7>, 2020.
- 656 Chen, C., Park, T., Wang, X., Piao, S., Xu, B., Chaturvedi, R. K., Fuchs, R., Brovkin,
657 V., Ciais, P., Fensholt, R., Tømmervik, H., Bala, G., Zhu, Z., Nemani, R. R., and
658 Myneni, R. B.: China and India lead in greening of the world through land-use
659 management, *Nat Sustain*, 2, 122–129, <https://doi.org/10.1038/s41893-019-0220-7>,
660 2019.
- 661 Chen, S., Fu, Y. H., Geng, X., Hao, Z., Tang, J., Zhang, X., Xu, Z., and Hao, F.:
662 Influences of Shifted Vegetation Phenology on Runoff Across a Hydroclimatic
663 Gradient, *Front. Plant Sci.*, 12, 802664, <https://doi.org/10.3389/fpls.2021.802664>, 2022.
- 664 Cheng, L., Zhang, L., Wang, Y.-P., Canadell, J. G., Chiew, F. H. S., Beringer, J., Li, L.,
665 Miralles, D. G., Piao, S., and Zhang, Y.: Recent increases in terrestrial carbon uptake
666 at little cost to the water cycle, *Nat Commun*, 8, 110, <https://doi.org/10.1038/s41467-017-00114-5>, 2017.
- 668 Cheng, W., Dan, L., Deng, X., Feng, J., Wang, Y., Peng, J., Tian, J., Qi, W., Liu, Z.,
669 Zheng, X., Zhou, D., Jiang, S., Zhao, H., and Wang, X.: Global monthly gridded
670 atmospheric carbon dioxide concentrations under the historical and future scenarios,
671 *Sci Data*, 9, 83, <https://doi.org/10.1038/s41597-022-01196-7>, 2022.
- 672 Fu, J., Liu, B., Wang, W., and Fei, E. X.: Evaluating main drivers of runoff changes
673 across China from 1956 to 2000 by using different budyko-based elasticity methods,
674 *Journal of Environmental Management*, 329, 117070,
675 <https://doi.org/10.1016/j.jenvman.2022.117070>, 2023.
- 676 Gan, G., Liu, Y., and Sun, G.: Understanding interactions among climate, water, and
677 vegetation with the Budyko framework, *Earth-Science Reviews*, 212, 103451,
678 <https://doi.org/10.1016/j.earscirev.2020.103451>, 2021.
- 679 Gutman, G. and Ignatov, A.: The derivation of the green vegetation fraction from
680 NOAA/AVHRR data for use in numerical weather prediction models, *International*
681 *Journal of Remote Sensing*, 19, 1533–1543, <https://doi.org/10.1080/014311698215333>,
682 1998.
- 683 He, J., Yang, K., Tang, W., Lu, H., Qin, J., Chen, Y., and Li, X.: The first high-
684 resolution meteorological forcing dataset for land process studies over China, *Sci Data*,
685 7, 25, <https://doi.org/10.1038/s41597-020-0369-y>, 2020.

- 686 Howell, T. A. and Dusek, D. A.: Comparison of Vapor-Pressure-Deficit Calculation
687 Methods—Southern High Plains, *J. Irrig. Drain Eng.*, 121, 191–198,
688 [https://doi.org/10.1061/\(ASCE\)0733-9437\(1995\)121:2\(191\)](https://doi.org/10.1061/(ASCE)0733-9437(1995)121:2(191)), 1995.
- 689 Jia, Y., Li, C., Yang, H., Yang, W., and Liu, Z.: Assessments of three
690 evapotranspiration products over China using extended triple collocation and water
691 balance methods, *Journal of Hydrology*, 614, 128594,
692 <https://doi.org/10.1016/j.jhydrol.2022.128594>, 2022.
- 693 Jiao, Y., Lei, H., Yang, D., Huang, M., Liu, D., and Yuan, X.: Impact of vegetation
694 dynamics on hydrological processes in a semi-arid basin by using a land surface-
695 hydrology coupled model, *Journal of Hydrology*, 551, 116–131,
696 <https://doi.org/10.1016/j.jhydrol.2017.05.060>, 2017.
- 697 Lammertsma, E. I., Boer, H. J. D., Dekker, S. C., Dilcher, D. L., Lotter, A. F., and
698 Wagner-Cremer, F.: Global CO₂ rise leads to reduced maximum stomatal conductance
699 in Florida vegetation, *Proc. Natl. Acad. Sci. U.S.A.*, 108, 4035–4040,
700 <https://doi.org/10.1073/pnas.1100371108>, 2011.
- 701 Li, B., Shi, X., Lian, L., Chen, Y., Chen, Z., and Sun, X.: Quantifying the effects of
702 climate variability, direct and indirect land use change, and human activities on runoff,
703 *Journal of Hydrology*, 584, 124684, <https://doi.org/10.1016/j.jhydrol.2020.124684>,
704 2020a.
- 705 Li, F., Xiao, J., Chen, J., Ballantyne, A., Jin, K., Li, B., Abraha, M., and John, R.: Global
706 water use efficiency saturation due to increased vapor pressure deficit, *Science*, 381,
707 672–677, <https://doi.org/10.1126/science.adf5041>, 2023.
- 708 Li, H., Shi, C., Zhang, Y., Ning, T., Sun, P., Liu, X., Ma, X., Liu, W., and Collins, A.
709 L.: Using the Budyko hypothesis for detecting and attributing changes in runoff to
710 climate and vegetation change in the soft sandstone area of the middle Yellow River
711 basin, China, *Science of The Total Environment*, 703, 135588,
712 <https://doi.org/10.1016/j.scitotenv.2019.135588>, 2020b.
- 713 Li, H., Cao, Y., Xiao, J., Yuan, Z., Hao, Z., Bai, X., Wu, Y., and Liu, Y.: A daily gap-
714 free normalized difference vegetation index dataset from 1981 to 2023 in China, *Sci*
715 *Data*, 11, 527, <https://doi.org/10.1038/s41597-024-03364-3>, 2024a.
- 716 Li, X., Xu, X., Sonnenborg, T. O., Andreasen, M., and He, C.: Effect of ecological
717 restoration on evapotranspiration and water yield in the agro-pastoral ecotone in
718 northern China during 2000–2018, *Journal of Hydrology*, 638, 131531,
719 <https://doi.org/10.1016/j.jhydrol.2024.131531>, 2024b.
- 720 Liang, L., Han, Z., Chen, W., Li, J., Liang, M., and Shen, S.: The source, transport,
721 deposition and direct radiative effect of mineral dust over western China: A modeling

722 study of July 2022 with focus on the Tibetan Plateau, *Atmospheric Research*, 311,
723 107708, <https://doi.org/10.1016/j.atmosres.2024.107708>, 2024.

724 Liu, C., Feng, S., Zhang, Q., Hu, J., Ma, N., Ci, H., Kong, D., and Gu, X.: Critical
725 influence of vegetation response to rising CO₂ on runoff changes, *Science of The Total*
726 *Environment*, 906, 167717, <https://doi.org/10.1016/j.scitotenv.2023.167717>, 2024.

727 Liu, J., Zhang, Q., Singh, V. P., and Shi, P.: Contribution of multiple climatic variables
728 and human activities to streamflow changes across China, *Journal of Hydrology*, 545,
729 145–162, <https://doi.org/10.1016/j.jhydrol.2016.12.016>, 2017.

730 Ma, T., Wang, T., Yang, D., and Yang, S.: Impacts of vegetation restoration on water
731 resources and carbon sequestration in the mountainous area of Haihe River basin, China,
732 *Science of The Total Environment*, 869, 161724,
733 <https://doi.org/10.1016/j.scitotenv.2023.161724>, 2023.

734 Medlyn, B. E., Duursma, R. A., Eamus, D., Ellsworth, D. S., Prentice, I. C., Barton, C.
735 V. M., Crous, K. Y., De Angelis, P., Freeman, M., and Wingate, L.: Reconciling the
736 optimal and empirical approaches to modelling stomatal conductance: RECONCILING
737 OPTIMAL AND EMPIRICAL STOMATAL MODELS, *Global Change Biology*, 17,
738 2134–2144, <https://doi.org/10.1111/j.1365-2486.2010.02375.x>, 2011.

739 Montibeller, B., Marshall, M., Mander, Ü., and Uuemaa, E.: Increased carbon
740 assimilation and efficient water usage may not compensate for carbon loss in European
741 forests, *Commun Earth Environ*, 3, 194, <https://doi.org/10.1038/s43247-022-00535-1>,
742 2022.

743 Mu, S., Zhou, S., Chen, Y., Li, J., Ju, W., and Odeh, I. O. A.: Assessing the impact of
744 restoration-induced land conversion and management alternatives on net primary
745 productivity in Inner Mongolian grassland, China, *Global and Planetary Change*, 108,
746 29–41, <https://doi.org/10.1016/j.gloplacha.2013.06.007>, 2013.

747 Nkiaka, E., Bryant, R. G., and Dembélé, M.: Quantifying Sahel Runoff Sensitivity to
748 Climate Variability, Soil Moisture and Vegetation Changes Using Analytical Methods,
749 *Earth Syst Environ*, 9, 491–504, <https://doi.org/10.1007/s41748-024-00464-3>, 2025.

750 Ogotu, B. O., D’Adamo, F., and Dash, J.: Impact of vegetation greening on carbon and
751 water cycle in the African Sahel-Sudano-Guinean region, *Global and Planetary Change*,
752 202, 103524, <https://doi.org/10.1016/j.gloplacha.2021.103524>, 2021.

753 Peng, H., Tague, C., and Jia, Y.: Evaluating the eco-hydrologic impacts of reforestation
754 in the Loess Plateau, China, using an eco-hydrologic model, *Ecohydrology*, 9, 498–513,
755 <https://doi.org/10.1002/eco.1652>, 2016.

- 756 Piao, S., Friedlingstein, P., Ciais, P., De Noblet-Ducoudré, N., Labat, D., and Zaehle,
757 S.: Changes in climate and land use have a larger direct impact than rising CO₂ on
758 global river runoff trends, *Proc. Natl. Acad. Sci. U.S.A.*, 104, 15242–15247,
759 <https://doi.org/10.1073/pnas.0707213104>, 2007.
- 760 Rahman, G., Farooq, U., Jung, M.-K., and Kwon, H.-H.: Spatiotemporal vegetation
761 dynamics in South Asia (2001-2023): roles of climate and anthropogenic activities,
762 *Geosci. Lett.*, 12, 31, <https://doi.org/10.1186/s40562-025-00403-8>, 2025.
- 763 Running, S. W., Thornton, P. E., Nemani, R., and Glassy, J. M.: Global Terrestrial
764 Gross and Net Primary Productivity from the Earth Observing System, in: *Methods in
765 Ecosystem Science*, edited by: Sala, O. E., Jackson, R. B., Mooney, H. A., and Howarth,
766 R. W., Springer New York, New York, NY, 44–57, [https://doi.org/10.1007/978-1-
4612-1224-9_4](https://doi.org/10.1007/978-1-
767 4612-1224-9_4), 2000.
- 768 Serrano-Notivoli, R., Martínez-Salvador, A., García-Lorenzo, R., Espín-Sánchez, D.,
769 and Conesa-García, C.: Rainfall–runoff relationships at event scale in western
770 Mediterranean ephemeral streams, *Hydrol. Earth Syst. Sci.*, 26, 1243–1260,
771 <https://doi.org/10.5194/hess-26-1243-2022>, 2022.
- 772 Shen, Q., Cong, Z., and Lei, H.: Evaluating the impact of climate and underlying
773 surface change on runoff within the Budyko framework: A study across 224 catchments
774 in China, *Journal of Hydrology*, 554, 251–262,
775 <https://doi.org/10.1016/j.jhydrol.2017.09.023>, 2017.
- 776 Sims, D. A., Rahman, A. F., Cordova, V. D., Baldocchi, D. D., Flanagan, L. B.,
777 Goldstein, A. H., Hollinger, D. Y., Misson, L., Monson, R. K., Schmid, H. P., Wofsy,
778 S. C., and Xu, L.: Midday values of gross CO₂ flux and light use efficiency during
779 satellite overpasses can be used to directly estimate eight-day mean flux, *Agricultural
780 and Forest Meteorology*, 131, 1–12, <https://doi.org/10.1016/j.agrformet.2005.04.006>,
781 2005.
- 782 Sun, W., Ding, X., Su, J., Mu, X., Zhang, Y., Gao, P., and Zhao, G.: Land use and cover
783 changes on the Loess Plateau: A comparison of six global or national land use and cover
784 datasets, *Land Use Policy*, 119, 106165,
785 <https://doi.org/10.1016/j.landusepol.2022.106165>, 2022.
- 786 Sun, X., Dong, Q., and Zhang, X.: Attribution analysis of runoff change based on
787 Budyko-type model with time-varying parameters for the Lhasa River Basin, Qinghai–
788 Tibet Plateau, *Journal of Hydrology: Regional Studies*, 48, 101469,
789 <https://doi.org/10.1016/j.ejrh.2023.101469>, 2023.
- 790 Tan, X., Tan, X., Liu, B., and Huang, Z.: Contribution of changes in vegetation
791 composition and climate variability on streamflow across the global watersheds,
792 *CATENA*, 232, 107394, <https://doi.org/10.1016/j.catena.2023.107394>, 2023.

793 Tan, X., Jia, Y., Yang, D., Niu, C., and Hao, C.: Impact ways and their contributions to
794 vegetation-induced runoff changes in the Loess Plateau, *Journal of Hydrology:*
795 *Regional Studies*, 51, 101630, <https://doi.org/10.1016/j.ejrh.2023.101630>, 2024.

796 Wang, D. L., Feng, H. M., Zhang, B. Z., Wei, Z., and Tian, Y. L.: Quantifying the
797 impacts of climate change and vegetation change on decreased runoff in china's yellow
798 river basin, *Ecohydrology & Hydrobiology*, 22, 310–322,
799 <https://doi.org/10.1016/j.ecohyd.2021.10.002>, 2022.

800 Wasko, C. and Sharma, A.: Global assessment of flood and storm extremes with
801 increased temperatures, *Sci Rep*, 7, 7945, <https://doi.org/10.1038/s41598-017-08481-1>,
802 2017.

803 Wei, H., Zhang, Y., Huang, Q., Chiew, F. H. S., Luan, J., Xia, J., and Liu, C.: Direct
804 vegetation response to recent CO₂ rise shows limited effect on global streamflow, *Nat*
805 *Commun*, 15, 9423, <https://doi.org/10.1038/s41467-024-53879-x>, 2024.

806 Xiao, M., Gao, M., Vogel, R. M., and Lettenmaier, D. P.: Runoff and
807 Evapotranspiration Elasticities in the Western United States: Are They Consistent With
808 Dooge's Complementary Relationship?, *Water Resources Research*, 56,
809 e2019WR026719, <https://doi.org/10.1029/2019WR026719>, 2020.

810 Xu, X., Yang, D., Yang, H., and Lei, H.: Attribution analysis based on the Budyko
811 hypothesis for detecting the dominant cause of runoff decline in Haihe basin, *Journal*
812 *of Hydrology*, 510, 530–540, <https://doi.org/10.1016/j.jhydrol.2013.12.052>, 2014.

813 Xu, Z., Jiang, Y., Jia, B., and Zhou, G.: Elevated-CO₂ Response of Stomata and Its
814 Dependence on Environmental Factors, *Front. Plant Sci.*, 7,
815 <https://doi.org/10.3389/fpls.2016.00657>, 2016.

816 Xue, B., A, Y., Wang, G., Helman, D., Sun, G., Tao, S., Liu, T., Yan, D., Zhao, T.,
817 Zhang, H., Chen, L., Sun, W., and Xiao, J.: Divergent Hydrological Responses to Forest
818 Expansion in Dry and Wet Basins of China: Implications for Future Afforestation
819 Planning, *Water Resources Research*, 58, e2021WR031856,
820 <https://doi.org/10.1029/2021WR031856>, 2022.

821 Yang, H. and Yang, D.: Derivation of climate elasticity of runoff to assess the effects
822 of climate change on annual runoff: DERIVATION OF CLIMATE ELASTICITY OF
823 RUNOFF, *Water Resour. Res.*, 47, <https://doi.org/10.1029/2010WR009287>, 2011.

824 Yang, H. and Yang, D.: Climatic factors influencing changing pan evaporation across
825 China from 1961 to 2001, *Journal of Hydrology*, 414–415, 184–193,
826 <https://doi.org/10.1016/j.jhydrol.2011.10.043>, 2012.

827 Yang, H., Xu, H., Huntingford, C., Ciais, P., and Piao, S.: Strong direct and indirect
828 influences of climate change on water yield confirmed by the Budyko framework,
829 *Geography and Sustainability*, 2, 281–287,
830 <https://doi.org/10.1016/j.geosus.2021.11.001>, 2021.

831 Yang, L., Zhao, G., Tian, P., Mu, X., Tian, X., Feng, J., and Bai, Y.: Runoff changes in
832 the major river basins of China and their responses to potential driving forces, *Journal*
833 *of Hydrology*, 607, 127536, <https://doi.org/10.1016/j.jhydrol.2022.127536>, 2022.

834 Yang, Y., Xiao, P., Feng, X., and Li, H.: Accuracy assessment of seven global land
835 cover datasets over China, *ISPRS Journal of Photogrammetry and Remote Sensing*, 125,
836 156–173, <https://doi.org/10.1016/j.isprsjprs.2017.01.016>, 2017.

837 Yang, Y., Roderick, M. L., Zhang, S., McVicar, T. R., and Donohue, R. J.: Hydrologic
838 implications of vegetation response to elevated CO₂ in climate projections, *Nature*
839 *Clim Change*, 9, 44–48, <https://doi.org/10.1038/s41558-018-0361-0>, 2019.

840 Zeng, F., Ma, M.-G., Di, D.-R., and Shi, W.-Y.: Separating the Impacts of Climate
841 Change and Human Activities on Runoff: A Review of Method and Application, *Water*,
842 12, 2201, <https://doi.org/10.3390/w12082201>, 2020.

843 Zhai, R. and Tao, F.: Climate Change in China Affects Runoff and Terrestrial
844 Ecosystem Water Retention More Than Changes in Leaf Area Index and Land
845 Use/Cover Over the Period 1982–2015, *JGR Biogeosciences*, 126, e2020JG005902,
846 <https://doi.org/10.1029/2020JG005902>, 2021.

847 Zhang, B., Tian, L., Zhao, X., and Wu, P.: Feedbacks between vegetation restoration
848 and local precipitation over the Loess Plateau in China, *Sci. China Earth Sci.*, 64, 920–
849 931, <https://doi.org/10.1007/s11430-020-9751-8>, 2021a.

850 Zhang C., WU C., KUAIS., PENG Z., Chang R., and ZHANG S.: Water-heat coupling
851 model-based study on runoff driving mechanism of Zhenjiangguan Watershed, *Water*
852 *Resources and Hydropower Engineering*, 53, 78–87,
853 <https://doi.org/10.13928/j.cnki.wrahe.2022.08.008>, 2022a.

854 Zhang, J., Zhang, Y., Sun, G., Song, C., Dannenberg, M. P., Li, J., Liu, N., Zhang, K.,
855 Zhang, Q., and Hao, L.: Vegetation greening weakened the capacity of water supply to
856 China’s South-to-North Water Diversion Project, *Hydrol. Earth Syst. Sci.*, 25, 5623–
857 5640, <https://doi.org/10.5194/hess-25-5623-2021>, 2021b.

858 Zhang, J., Zhang, Y., Sun, G., Song, C., Li, J., Hao, L., and Liu, N.: Climate Variability
859 Masked Greening Effects on Water Yield in the Yangtze River Basin During 2001–
860 2018, *Water Resources Research*, 58, e2021WR030382,
861 <https://doi.org/10.1029/2021WR030382>, 2022b.

862 Zhang, S., Yang, H., Yang, D., and Jayawardena, A. W.: Quantifying the effect of
863 vegetation change on the regional water balance within the Budyko framework,
864 Geophysical Research Letters, 43, 1140–1148, <https://doi.org/10.1002/2015GL066952>,
865 2016a.

866 Zhang, X., Zhao, T., Xu, H., Liu, W., Wang, J., Chen, X., and Liu, L.: GLC_FCS30D:
867 the first global 30 m land-cover dynamics monitoring product with a fine classification
868 system for the period from 1985 to 2022 generated using dense-time-series Landsat
869 imagery and the continuous change-detection method, Earth Syst. Sci. Data, 16, 1353–
870 1381, <https://doi.org/10.5194/essd-16-1353-2024>, 2024.

871 Zhang, Y., Song, C., Sun, G., Band, L. E., McNulty, S., Noormets, A., Zhang, Q., and
872 Zhang, Z.: Development of a coupled carbon and water model for estimating global
873 gross primary productivity and evapotranspiration based on eddy flux and remote
874 sensing data, Agricultural and Forest Meteorology, 223, 116–131,
875 <https://doi.org/10.1016/j.agrformet.2016.04.003>, 2016b.

876 Zhao, F., Wu, Y., Ma, S., Lei, X., and Liao, W.: Increased Water Use Efficiency in
877 China and Its Drivers During 2000–2016, Ecosystems, 25, 1476–1492,
878 <https://doi.org/10.1007/s10021-021-00727-4>, 2022.

879 Zhou, S., Yu, B., Huang, Y., and Wang, G.: The effect of vapor pressure deficit on
880 water use efficiency at the subdaily time scale, Geophysical Research Letters, 41, 5005–
881 5013, <https://doi.org/10.1002/2014GL060741>, 2014.

882 Zhou, S., Yu, B., Lintner, B. R., Findell, K. L., and Zhang, Y.: Projected increase in
883 global runoff dominated by land surface changes, Nat. Clim. Chang., 13, 442–449,
884 <https://doi.org/10.1038/s41558-023-01659-8>, 2023.

885
886